

Validation of the Yale Circumferential Quantification Method Using ^{201}Tl and $^{99\text{m}}\text{Tc}$: A Phantom Study

Suna Kirac, Frans J.Th. Wackers, and Yi-Hwa Liu

Section of Cardiovascular Medicine, Department of Internal Medicine, and the Cardiovascular Nuclear Imaging Laboratory, Department of Diagnostic Radiology, Yale University School of Medicine, New Haven, Connecticut

The Yale circumferential quantification (Yale CQ) method for quantification of SPECT images has been validated previously using empirically derived correction factors. In the present studies, the Yale CQ method was further validated using 2 SPECT gamma cameras and 2 radioisotopes. **Methods:** SPECT images were acquired from cardiac phantoms with multiple fillable inserts to simulate myocardial perfusion defects of varying extents and severities. Seventy phantom configurations were created. One hundred and forty SPECT images (70 with $^{99\text{m}}\text{Tc}$ and 70 with ^{201}Tl) were acquired using a triple-head SPECT camera. SPECT defects were quantified using the Yale CQ method, with incorporation of $^{99\text{m}}\text{Tc}$ - and ^{201}Tl -derived normal databases and correction factors. **Results:** Quantified phantom SPECT defect sizes acquired with $^{99\text{m}}\text{Tc}$ correlated well with actual calculated defect sizes ($r = 0.96$, $y = 0.92x - 0.41$). Bland-Altman analysis of agreement revealed strong agreement over a wide range of defect sizes, with a mean error of 1.2% and 2 SDs of 5.0%. Overall ^{201}Tl SPECT defect sizes also correlated well with actual defect sizes ($r = 0.92$), but there was a systematic underestimation ($y = 0.72x - 0.76$). Bland-Altman analysis showed underestimation over the entire range of defect sizes, with a mean error of 3.4% and 2 SDs of 7.5%. Implementation of a normal ^{201}Tl phantom database improved accuracy of quantification ($r = 0.95$, $y = 0.87x - 1.36$). The addition of ^{201}Tl -specific correction factors further improved accuracy ($r = 0.94$, $y = 0.98x - 1.52$). Reproducibility of SPECT defect sizes quantification for $^{99\text{m}}\text{Tc}$ using 2 gamma cameras was excellent ($r = 0.98$, $y = 0.98x + 0.84$). **Conclusion:** The Yale CQ SPECT quantification method, using the empirically derived correction factors, provides accurate and reproducible quantification of phantom defects over a wide range of defect sizes. Accurate quantification of ^{201}Tl and $^{99\text{m}}\text{Tc}$ SPECT defect sizes requires radiotracer-specific normal databases.

Key Words: SPECT quantification; Yale CQ method; phantom validation

J Nucl Med 2000; 41:1436-1441

Extensive clinical evidence exists to show that the severity and extent of stress-induced radionuclide myocar-

dial perfusion abnormalities provide important prognostic information in patients with known or suspected coronary artery disease. Therefore, accurate and reproducible quantification of myocardial perfusion abnormalities is of substantial clinical relevance. Polar maps (1,2) and circumferential count profiles (3-5) are widely used for quantification in cardiac SPECT images. These quantification algorithms are based on either maximal or mean counts in SPECT-reconstructed slices (6-9). The Yale circumferential quantification (Yale CQ) method is based on circumferential count distribution profiles derived from reconstructed SPECT slices. This method has been used for over a decade in our laboratory for routine quantification of SPECT myocardial perfusion abnormalities (5,8,10). The accuracy of this quantification method was evaluated previously in $^{99\text{m}}\text{Tc}$ -filled phantoms with defect inserts. Using empirically derived correction factors and normal databases, SPECT quantification of phantom defects was found to be accurate and reproducible (5).

In this study, the accuracy and reproducibility of the Yale CQ method are further validated in phantoms using different SPECT gamma cameras and different radiopharmaceuticals (i.e., $^{99\text{m}}\text{Tc}$ - and ^{201}Tl -filled phantoms).

MATERIALS AND METHODS

Phantoms

An elliptical lung-spine body phantom (model ECT/LUNG/P; Data Spectrum, Hillsborough, NC) with a cardiac insert was used in this study. The cardiac insert consisted of a central bullet-shaped cylinder simulating the left ventricular (LV) cavity and a space between the central cylinder and the hollow cylinder simulating the LV myocardium (Fig. 1). The volume of the simulated LV myocardium was 125 mL.

The thoracic and the central cylinder of the cardiac phantom were filled with water to simulate uniform attenuation of thoracic organs and the LV blood pool. The hollow cardiac chamber simulating the LV myocardium was filled with a well-mixed radioisotope solution of a concentration of 0.092 MBq/mL (2.5 $\mu\text{Ci/mL}$), representing normal "myocardial" perfusion. To simulate myocardial perfusion defects of different extents, defect inserts with volumes of 5, 10, and 20 mL (model ECT/FIL/I; Data Spectrum) were used. Subsequently, defects with sizes ranging from 0% to 32% of the simulated LV volume were created. Defect

Received Jul. 8, 1999; revision accepted Apr. 6, 2000.

For correspondence or reprints contact: Yi-Hwa Liu, PhD, Division of Cardiovascular Medicine, Department of Internal Medicine, Yale University School of Medicine, New Haven, CT 06520-8017.

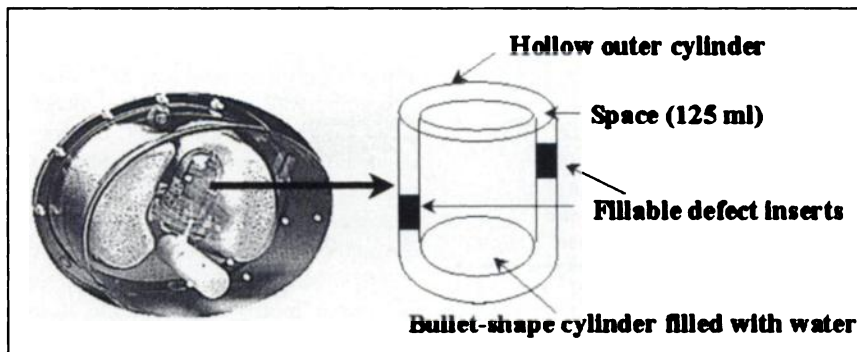


FIGURE 1. Elliptical lung–spine body phantom and cardiac insert. Hollow 125-mL space simulating the LV myocardium was filled with 0.092 MBq/mL (2.5 μ Ci/mL) (normal concentration) ^{99m}Tc or ^{201}Tl . Defect inserts were filled with variable concentrations of normal—100%, 80%, 60%, 40%, 20%, 5%, and 0%—to mimic normal perfusion (100%) and perfusion abnormalities of varying defect severities. Using fillable defect inserts of varying volumes, and by combining multiple inserts, perfusion abnormalities of varying defect extents can be simulated (see text and Tables 1 and 2).

volumes of 40 mL (32% of simulated LV) and 30 mL (24% of simulated LV) were created by combining multiple inserts. To simulate myocardial perfusion defects of different severities, the defect inserts were filled with ^{99m}Tc or ^{201}Tl solutions of varying concentrations, ranging from 0% to 100% of the normal concentration (Table 1). Seventy phantom configurations (Table 2) were created by positioning defects in the anterior or inferior walls of the simulated LV myocardium, by positioning 1 or multiple defect inserts in the simulated LV myocardium, and by using different isotope solutions. There were 28 phantom configurations with pure anterior defects and 28 with pure inferior defects. In the remaining 14 phantom configurations, large defects were created by combining multiple inserts simultaneously in the anterior and inferior locations (Table 3). To assess the reproducibility of SPECT quantification, 30 phantom defect configurations used in our previous study were re-created, and SPECT acquisitions were repeated on the same camera (camera 2) for a second time and also on a different camera (camera 1) (Table 3).

Calculation of Actual Defect Size

Actual myocardial perfusion defect size was calculated using the formula defined previously (5) from the total simulated LV volume, the defect insert(s) volume, and radioisotope concentration:

$$\text{Actual defect size} = (1 - C) \times V, \quad \text{Eq. 1}$$

where C = concentration of radioisotope solution in the defect insert, represented as percentage of the normal solution, and V = defect insert volume, represented as percentage of the simulated LV myocardium.

Image Acquisition

One hundred and forty SPECT phantom images were acquired (Table 2), with ^{99m}Tc (70 acquisitions) or ^{201}Tl (70 acquisitions), using a triple-head SPECT camera (camera 1). In addition, 30 SPECT phantom images (Table 3) were acquired on another triple-head SPECT camera (camera 2), which was used in our previous study (5). Both cameras were the same brand (Prism 3000; Picker International, Bedford Heights, OH) and equipped with low-energy–high-resolution, parallel-hole collimators. Sixty projections were acquired in a continuous acquisition mode over a 360° arc and 45 s/angle, in a 64 \times 64 matrix, and a pixel size of 5.3 mm. A 15% energy window at 140 keV photo-peak was used for ^{99m}Tc SPECT imaging. For ^{201}Tl SPECT imaging, 2 energy windows (40% at 76 keV and 20% at 167 keV) were used.

Image Reconstruction and Filtering

Tomographic images were reconstructed using standard filtered backprojection and Butterworth low-pass filtering (order of 4.0 and cutoff of 0.23 Nyquist frequency). Short- and long-axis SPECT slices were generated perpendicular to the axes of the cardiac phantom. No attenuation correction or scatter correction was used during processing.

SPECT Quantification

Slice Selection. Circumferential maximal count profiles were generated from operator-selected short-axis slices and representative horizontal long-axis slices. The short-axis slices included for quantification were selected from slices between the apex and the

TABLE 1
Phantom Defect Configurations

Variables of defect configuration	Camera 1 (70 configurations)		Camera 2 (30 configurations)	
	^{99m}Tc	^{201}Tl	^{99m}Tc	^{99m}Tc
Radioactive isotopes	^{99m}Tc	^{201}Tl	^{99m}Tc	^{99m}Tc
Isotope concentrations (% normal)	0, 5, 20, 40, 60, 80, 100	0, 5, 20, 40, 60, 80, 100	0, 100	5, 20, 40, 60, 80
Defect volumes (% of simulated LV myocardium)	4, 8, 16, 24, 32	4, 8, 16, 24, 32	4, 8, 16, 24, 32	8

Phantom defect configurations were created using 2 radioisotopes, different radioisotope concentrations, different locations (anterior and inferior), and different defect volumes. Seventy configurations for each radioisotope were imaged on camera 1, and 30 configurations for ^{99m}Tc were imaged on camera 2.

TABLE 2
Number of Radioisotope Concentrations Using Camera 1
Defect Configurations

Defect volume (% of simulated LV myocardium)	Defect location				Total
	Anterior	Inferior	Anterior	Anterior	
			basal and inferior apical	apical and inferior basal	
4	7	7	0	0	14
8	7	7	0	0	14
16	7	7	0	0	14
24	7	7	0	0	14
32	0	0	7	7	14
Total	28	28	7	7	70

Seventy configurations of ^{99m}Tc - or ^{201}Tl -filled phantoms were created for imaging with camera 1, using defects of different volumes, different radioisotope concentrations, and different locations.

base of the simulated left ventricle. The first apical slice used for quantification was defined as the first apical slice showing the cavity of the simulated left ventricle. The last basal slice used for quantification was defined as the last basal slice in which the image became fuzzy. The most apical and most basal slices thus defined were excluded from quantification to minimize the partial volume effect in the apex and the boundary slice of the simulated left ventricle at the base. More specifically, the adjacent slices to the first apical slice and the last basal slice as defined above were selected for quantification. For quantification of the apex, 4 operator-selected, central horizontal, long-axis slices were used.

Detection of Centers and Edges in Selected Short-Axis Slices. We have previously described our automatic approach for finding the centers and edges of the selected short axis slices (5). In the Yale CQ software (Yale University, New Haven, CT), the centers and edges can be defined manually by operator interaction using a programmed user-graphical interface. Calculation of the LV volume excluding the apex is based on the automatically or manually defined inner and outer edges of the short-axis slices.

TABLE 3
Number of Radioisotope Concentrations Using Camera 2
Defect Configurations

Defect volume (% of simulated LV myocardium)	Defect location				Total
	Anterior	Inferior	Anterior	Anterior	
			basal and inferior apical	apical and inferior basal	
4	2	2	0	0	4
8	7	7	0	0	14
16	2	2	0	0	4
24	2	2	0	0	4
32	0	0	2	2	4
Total	13	13	2	2	30

Thirty configurations of ^{99m}Tc -filled phantom were created for imaging with camera 2, using defects of different volumes, different radioisotope concentrations, and different locations.

Delineation of the Apex. For quantification of the apex, the 4 central horizontal axis slices were averaged. A rectangle was manually positioned and resized to circumscribe the simulated LV myocardial wall in the averaged image for determination of the center and radius of the apex (5). To be consistent with the shape assumption as applied to the short-axis slices, the apex was assumed to have a shape of semispherical shell. The uniform thickness of the myocardium assumed for the short-axis slices was also applied to the apex to facilitate defect size calculation.

Interpolation of the Slices and Edges. The selected short-axis slices were linearly interpolated to 36 slices. The center locations and the radii of the circular edges were interpolated in the same way. Interpolation was not applied to the 4 central horizontal long-axis slices, because the number of the horizontal long-axis slices selected for the apex quantification was fixed (i.e., always 4).

Generation of Circumferential Profile. Circumferential count profiles were generated slice by slice. Each of the 36 interpolated slices was divided into 128 radial sectors using the polar transformation. A circumferential count profile was generated from the maximal pixel values in each of the 128 radial sectors. Consequently, 36 maximal count profiles, each with 128 data points, were created. Each of these 128-point profiles was in turn divided into 4 anatomical zones: anterior, septal, inferior, and lateral. For the generation of a circumferential profile from the apex, the averaged apical region of 4 central horizontal, long-axis slices was divided into sectors using the same spatial sampling frequency as for the short-axis slices. The apical region was divided into 3 anatomical zones: septal, apical, and lateral. A circumferential count profile was then generated as described above. However, only the portion of the profile within the apical zone was used for quantification. Each circumferential count profile was normalized to the highest count value, which was thus represented as 100%. This normalization of individual circumferential profiles was chosen because no attenuation correction was applied during reconstruction.

Normal Data Files. Normal data files were generated for each phantom configuration by SPECT imaging of the lung-spine body phantom, with the defect inserts filled with 0.092 MBq/mL (2.5 $\mu\text{Ci/mL}$; 100% concentration) ^{99m}Tc . The lower limits of normal for the phantom images were calculated as mean minus 2 SDs of the normal profiles.

Calculation of SPECT Defect Size. In each slice, SPECT defect size was defined as the area between the derived circumferential count profile and the lower limit of normal, divided by the summation of that defect area and the area below the derived count profile (5). SPECT defect size for the apex was calculated separately. The calculated defect sizes were further scaled by a weighting factor on basis of the radii of the slices and then integrated into a global defect size. Ultimately, global phantom defect size in all slices was calculated as a global volume-weighted defect size.

Empirical Correction for Underestimation of Defect Size. The volume-weighted SPECT defect size is inevitably an underestimation of the actual defect size, because of the limited resolution of the SPECT imaging system and the use of 3-dimensional, low-pass filtering on the SPECT images. The correction factors for ^{99m}Tc used in this study were empirically determined in our previous study (5), whereas for ^{201}Tl , the correction factors were computed from the linear regression equation of phantom data of defect inserts of varying sizes without ^{201}Tl content (0% concentration).

Statistical Analysis. Linear regression analysis (11) was used to assess the correlation of the defect sizes with actual known defect

sizes and reproducibility of quantification. Bland-Altman analysis of agreement (12) was used to demonstrate the estimation errors in the quantified defect sizes. The estimation error of the defect size was defined as a difference between the SPECT quantified defect size and the actual defect size and was represented as percentage of the total simulated LV myocardium.

RESULTS

^{99m}Tc-Filled Phantoms

Overall, quantified SPECT defect sizes of the 70 ^{99m}Tc-filled phantom configurations, using camera 1 and the predefined correction factors and ^{99m}Tc normal reference profiles, showed a good correlation ($r = 0.96$) with the calculated actual sizes of the phantom defect inserts (Fig. 2A). Similarly, Bland-Altman analysis of agreement (Fig. 2B) demonstrated good accuracy over the entire range of defect sizes, with a mean error of 1.2% of the simulated LV and 2 SDs of the mean error being 5.0% of the simulated LV.

²⁰¹Tl-Filled Phantoms

Overall, quantified SPECT defect sizes of 70 ²⁰¹Tl-filled phantom configurations, using camera 1, the previously defined correction factors, and normal phantom database

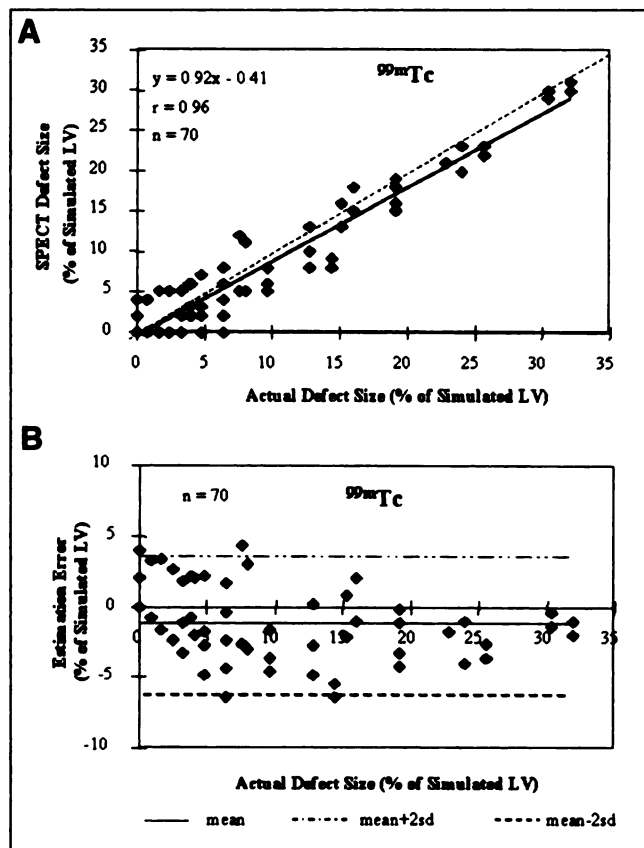


FIGURE 2. Results of SPECT quantification of ^{99m}Tc-filled phantom defect sizes using SPECT camera 1. (A) Correlation of quantified SPECT defect size with actual calculated size of cardiac defect insert. (B) Bland-Altman analysis of agreement and estimated error between quantified SPECT defect size and actual defect insert size. Dashed line represents line of identity.

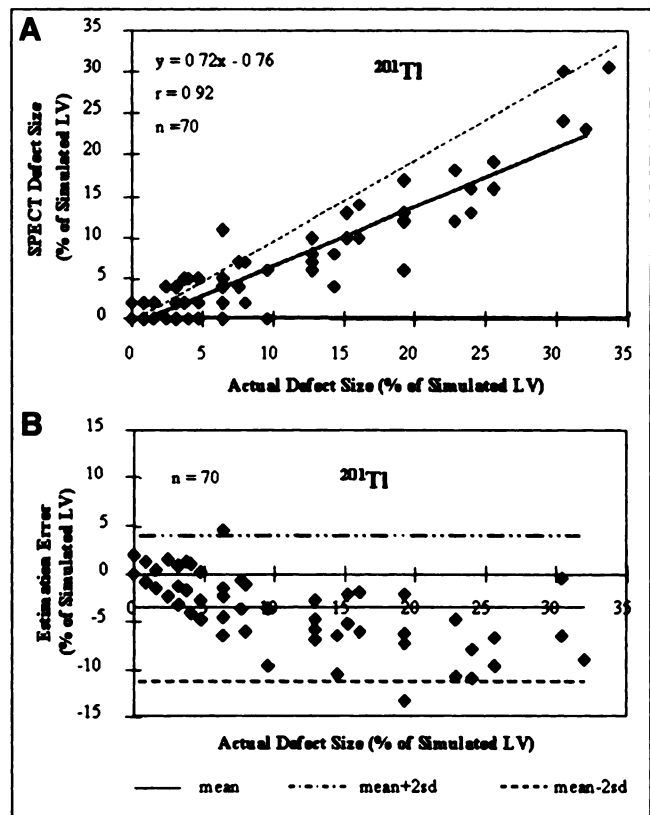


FIGURE 3. Results of SPECT quantification of ²⁰¹Tl-filled phantom defect sizes using ^{99m}Tc normal database and ^{99m}Tc-derived correction factors. (A) Correlation of SPECT defect size with actual calculated defect size. (B) Bland-Altman analysis of agreement and estimated error between quantified SPECT defect size and actual defect size.

(reference profiles) derived from ^{99m}Tc-filled phantoms, showed a strong correlation ($r = 0.92$) with the actual defect sizes (Fig. 3A). However, there was a systematic underestimation of SPECT quantified defect sizes. Bland-Altman analysis of agreement (Fig. 3B) confirmed an underestimation over the entire range of defect sizes. The mean error was 3.4% of the simulated LV, and 2 SDs of the error was 7.5% of the simulated LV (Fig. 3B).

Using new reference normal profiles derived from imaging ²⁰¹Tl-filled normal phantoms, the underestimation of the quantified SPECT defect sizes improved (Fig. 4A). The mean error of the simulated LV was 2.6%, and 2 SDs of the error was 5.8% of the simulated LV (Fig. 4B). Slight improvement in the slope of correlation line (0.98 vs. 0.87) and in the mean error (1.7% vs. 2.6%) was achieved by the addition of a new ²⁰¹Tl-specific correction factors (Fig. 5). However, as seen in Figure 5B, there was no improvement in the variation of the data when the new ²⁰¹Tl-specific correction factor was used.

Reproducibility of SPECT Quantification

Thirty ^{99m}Tc-filled phantom configurations were imaged with both cameras 1 and 2 (Table 2). As shown in Figure 6A, agreement of the SPECT quantification using 2 SPECT

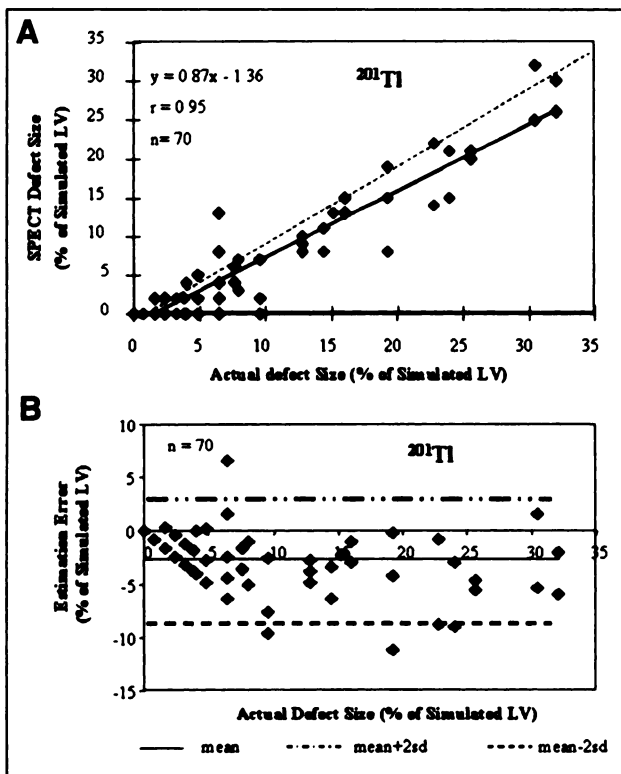


FIGURE 4. Results of SPECT quantification of ^{201}Tl -filled phantom defect sizes using ^{201}Tl normal database and $^{99\text{m}}\text{Tc}$ -derived correction factors. (A) Correlation of SPECT defect size with actual calculated defect size. (B) Bland-Altman analysis of agreement and estimated error between quantified SPECT defect size and actual defect size.

cameras was excellent ($r = 0.98$). Reproducibility of the creation of 30 phantom configurations and of quantification of SPECT defect sizes in this study was compared with the results reported in the previous study (5), and this correlation was also very good, as demonstrated in Figure 6B ($r = 0.98$).

DISCUSSION

The present phantom study further validates the Yale CQ SPECT quantification method using 2 cameras, 2 radioisotopes, and a wide range of phantom defect sizes and severities. Using empirically derived correction factors, quantification of phantom defects was accurate and reproducible. We reported previously that $^{99\text{m}}\text{Tc}$ -sestamibi and ^{201}Tl normal patient databases were not statistically different, although they were not identical (13). This study indicates that for accurate SPECT quantification, it is necessary to use radiotracer-specific normal databases and correction factors. Quantified SPECT phantom defect sizes correlated well with the actual calculated sizes of defect inserts when correction factors were incorporated into the quantification.

Photon attenuation and scatter may have an important role in the accuracy of SPECT image quantification. Because of attenuation, apical slices always had lower counts than basal slices in normal phantoms. To avoid this confounding factor

in quantification, each reconstructed slice was normalized to itself.

The agreement between quantified SPECT defect size and actual defect size may be dependent on the SPECT image resolution. Also, the effect of low-pass filtering should be considered. Specifically, underestimation or overestimation may occur when SPECT quantification is based on maximal sectorial counts rather than mean counts (6,7). Using radiotracer-specific software adjustments, a Bland-Altman analysis of agreement showed good accuracy and reproducibility using different gamma cameras.

The main limitation of this study is the use of phantoms. Human myocardial infarction or stress-induced myocardial perfusion abnormalities are imperfectly imitated by fillable defect inserts in a cardiac phantom. Phantom images with defect inserts do not closely mimic human myocardial perfusion defects. Nevertheless, the advantage of a phantom study is that the extent (size of insert) and severity (radiotracer concentration) of defects can be exactly calculated.

We encountered a confounding factor in using phantoms as truthful benchmarks for quantification. Circumferential count profiles of a normal cardiac phantom were not the anticipated straight line. Instead, the normal phantom circum-

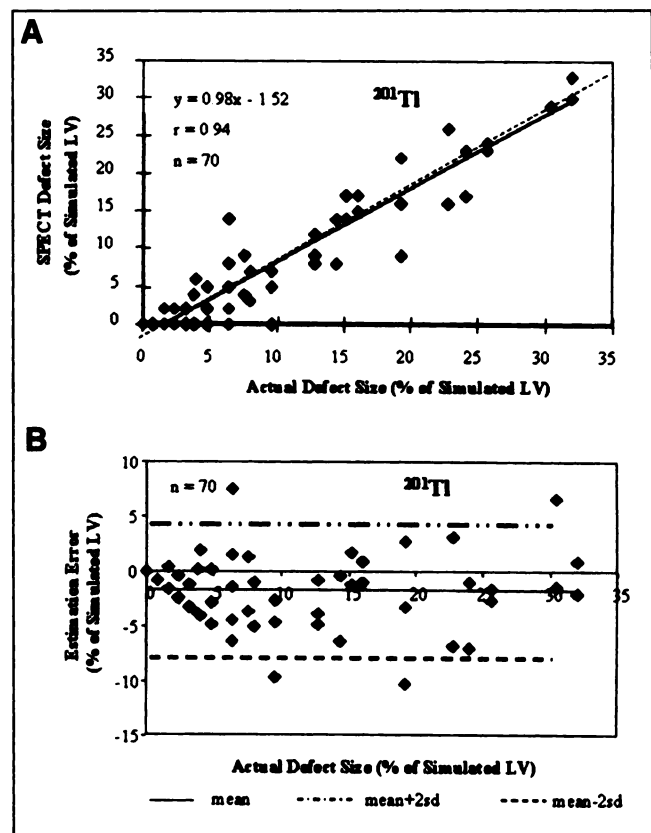


FIGURE 5. Results of SPECT quantification of ^{201}Tl -filled phantom defect sizes using ^{201}Tl normal database and ^{201}Tl -derived correction factors. (A) Correlation of SPECT defect size with actual calculated defect size. (B) Bland-Altman analysis of agreement and estimated error between quantified SPECT defect size and actual defect size.

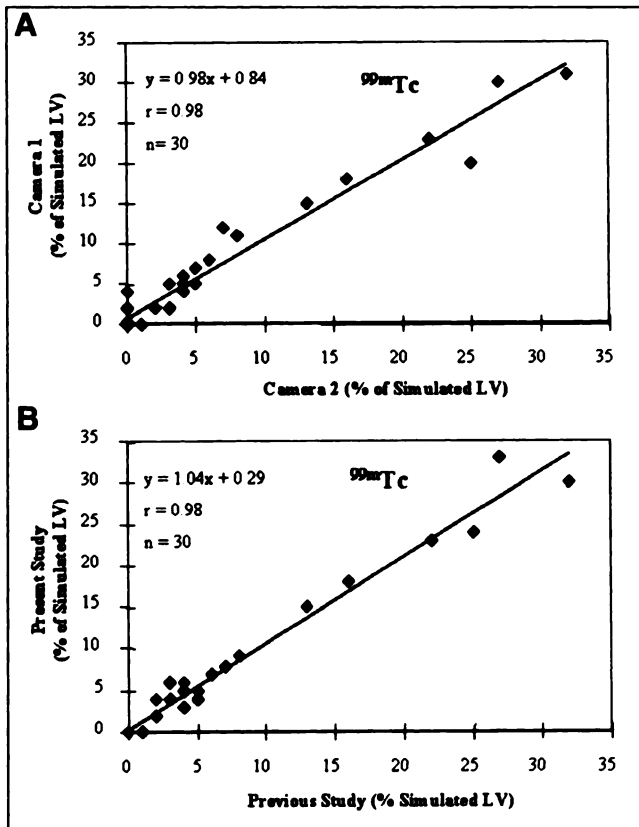


FIGURE 6. Reproducibility of quantified SPECT defect sizes for 30 ^{99m}Tc -filled phantom configurations. (A) Reproducibility of SPECT quantification of images acquired from cameras 1 and 2. (B) Reproducibility of re-creation of 30 phantom configurations and SPECT quantification of images in this study and in previously reported study (5).

ferential count profiles were lower in the inferior wall, presumably because of self-attenuation of the phantom. Moreover, cardiac inserts filled with 100% concentration of radiotracer also showed evidence of self-attenuation. Consequently, it was necessary to establish normal profiles for each phantom configuration. Therefore, this study should be repeated in the future, with the application of attenuation correction, scatter correction, and resolution compensation.

We found excellent agreement between quantification of SPECT phantom images acquired on 2 gamma cameras of the same brand. Whether this also applies to gamma cameras

of different manufacturers is unclear. This was not tested in this study.

CONCLUSION

SPECT quantification using the Yale CQ method is highly reproducible and accurate in accessing myocardial perfusion abnormalities using different gamma cameras of the same brand. Radiotracer-specific normal databases and correction factors are required to improve the systematic underestimation of the defect sizes.

ACKNOWLEDGMENT

Drs. Wackers and Liu, through an arrangement with Yale University (New Haven, CT), receive royalties from the sale of Yale CQ software.

REFERENCES

1. Nuyts J, Mortelmans L, Suetens P, Oosterlinck A, de Roo M. Model-based quantification of myocardial perfusion images from SPECT. *J Nucl Med.* 1989; 30:1992-2001.
2. Zaret BL, Wackers FJTh. Nuclear cardiology. *N Engl J Med.* 1993;329:775-783.
3. Burrow RD, Pond M, Schafer AW, Becker L. "Circumferential profiles:" a new method for computer analysis of thallium-201 myocardial perfusion images. *J Nucl Med.* 1979;20:771-777.
4. O'Connor MK, Gibbons RJ, Juni JE, O'Keefe J, Ali A. Quantitative myocardial SPECT for infarct sizing: feasibility of a multicenter trial evaluated using a cardiac phantom. *J Nucl Med.* 1995;36:1130-1136.
5. Liu YH, Sinusas AJ, Deman P, Zaret BL, Wackers FJTh. Quantification of single-photon emission computerized tomographic myocardial perfusion images: methodology and validation of the Yale-CQ method. *J Nucl Cardiol.* 1999;6:190-203.
6. Garcia EV, Van Train K, Maddahi J, et al. Quantification of rotational thallium-201 myocardial tomography. *J Nucl Med.* 1985;26:17-26.
7. Prigent F, Maddahi J, Garcia EV, et al. Comparative methods for quantifying myocardial infarct size by thallium-201 SPECT. *J Nucl Med.* 1987;28:325-333.
8. Liu YH, Sinusas AJ, Shi CQX, et al. Quantification of technetium 99m-labeled sestamibi single-photon emission computed tomography based on mean counts improves accuracy for assessment of relative myocardial blood flow: experimental validation in a canine model. *J Nucl Cardiol.* 1996;3:312-320.
9. Faber TL. Tomographic imaging: methods. In: Gerson MC, ed. *Cardiac Nuclear Medicine.* New York: McGraw-Hill; 1997:53-81.
10. Liu YH, Sinusas AJ, Wackers FJTh. Validation of a new SPECT quantification method using computer simulation. In: Moonier PA, ed. *Conference Record of the 1995 IEEE/MIC.* Piscataway, NJ: IEEE Service Center; 1995:1506-1509.
11. Ingelfinger JA, Mosteller F, Thibodeau LA, Ware JH. *Biostatistics in Clinical Medicine.* New York: McGraw-Hill; 1994:193-224.
12. Bland M, Altman DG. Statistical methods for assessing agreement between two methods of clinical measurement. *Lancet.* 1986;1:307-310.
13. Naruse H, Daher E, Sinusas A, et al. Quantitative comparison of planar and SPECT normal data files of thallium-201, technetium-99m-sestamibi, technetium-99m-tetrofosmin and technetium-99m-furifosmin. *J Nucl Med.* 1996;37:1783-1788.